ELSEVIER

A direct boundary-layer stability analysis of steady-state cavity convection flow

S. Armfield and R. Janssen
School of Civil Engineering, The University of New South Wales, Sydney, NSW, Australia

Natural convection flow in cavities with insulated top and bottom and heated and cooled walls is known to exhibit travelling wave instabilities in the thermal boundary layers that form on the walls. In water (Pr=7.5) at Rayleigh number $Ra=6\times10^8$, these waves have been observed at start-up. However no such waves have been observed for the fully developed flow, although it may be assumed that the stability character of the boundary layers is at least approximately the same. The start-up waves are generated by perturbations to the system. In the present paper, an artificial perturbation is applied to the system to determine the stability character of the boundary layers in fully developed flow. It is shown that the thermal boundary layers in the fully developed flow have approximately the same stability character as the start-up flow. © *1996 by Elsevier Science Inc.*

Keywords: natural convection; stability; thermal boundary layer; numerical simulation

Introduction

When the opposing walls of a cavity, with insulated top and bottom containing a stationary and isothermal fluid, are heated and cooled to $T_m + \Delta T/2$ and $T_m - \Delta T/2$, where T_m is the mean temperature of the fluid, thermal boundary layers are generated on each of the walls. The thermal boundary layers eject heated and cooled jets onto the ceiling and floor, respectively, which form stable intrusions that transit the cavity. When the intrusions reach the far wall, they are partly entrained by the boundary layer there, with the unentrained fluid filling the cavity, ultimately leading to a stratified interior at long time. The reader is referred to Patterson and Armfield (1990) for a full description of the flow.

For the flow in a square cavity with Rayleigh number $Ra = 6\times10^8$ and Prandtl number $Pr = 7.5$, during the initial transient, two packets of unstable travelling waves are observed to transit up the hot wall and down the cold wall. The initial packet of waves is associated with the start up of the thermal boundary layers, while the latter is associated with the intrusion from the far wall striking and perturbing the base of the thermal boundary layer (Armfield 1989; Patterson and Armfield 1990; Armfield and Patterson 1992).

In Armfield and Patterson (1992) a linearised stability analysis was presented for the vertical boundary layer during the time at which the travelling wave packets referred to above are observed. The stability analysis showed that the boundary layers will support travelling wave modes, and that above a critical point on the hot wall, and below a critical point on the cold wall, the boundary layers will be unstable for a narrow band of wave-numbers. This is consistent with the observed behaviour of the wave-packets (Armfield and Patterson 1992). It was suggested that the initial wave packet is generated by the singularity that originates at the base of the hot wall at start-up. The wave packet is then dispersed, with selected modes decaying and amplifying as they travel up the boundary layer according to the local stability characteristics. The second packet, as noted above, is generated by the perturbation resulting from the intrusion striking the base of the thermal boundary layer. The boundary layers during the initial transient for the cavity were shown to have equivalent stability characteristics to the boundary layers on a semi-infinite vertical heated plate.

After the passage of the second set of boundary-layer waves, no further travelling wave activity is observed at the Rayleigh number considered, although it may be assumed that during the resulting transition phase and at steady state, the boundary layer still has approximately the same stability characteristics as it had during start-up. That is, if the system is perturbed with an appropriate signal, the boundary layer would respond by exhibiting waves travelling downstream from the point of perturbation, and above a certain critical height on the wall, amplifying in the direction of travel. It is also well known that for lower Prandtl number flows ($Pr \sim 1$) and for $Pr \sim 7$ flows in high aspect ratio cavities, above a critical Rayleigh number, a bifurcation with a single frequency occurs with travelling boundary layer waves of the type observed during the initial transient as described above (LeQuéré and Alziary de Roquefort 1985; LeQuéré 1990). It is not clear why such a bifurcation with a single frequency does not seem to occur for the long time $Pr \sim 7$ flow in the square cavity (Janssen and Henkes 1995). Similarly, it is not known why the critical Rayleigh numbers for the cavity flows which do exhibit a bifurcation with the characteristics of the boundary-layer waves, are always orders-of-magnitude greater than the critical Rayleigh number for the equivalent semi-infinite plate.

In the present paper, the stability of the steady-state cavity thermal boundary layers at $Pr = 7.5$ is examined directly by including a perturbation at the base of the hot wall. Both random

Address reprint requests to Steven Armfield, Mechanical and Mechatronic Engineering, The University of Sydney, Sydney 2006, NSW, Australia.

Received 21 November 1994; accepted 18 May 1996

Int. J. Heat and Fluid Flow 17: 539–546, 1996

655 Avenue of the Americas, New York, NY 10010

0142-727X/96/$15.00
PII S0142-727X(96)00065-1

and single-mode perturbations have been introduced. Introducing the random perturbation allows the response to a broadband signal to be determined, and specifically the critical Rayleigh number and frequency to be approximately identified. The single-mode perturbation then allows the amplification, wave speed, and critical Rayleigh number for that mode to be accurately determined. The steady-state boundary layer is seen to have a critical height below which all modes decay and above which a band of modes becomes unstable and begins to grow. This results in the boundary layer acting as a band-pass filter for a small range of frequencies, in the same manner as the boundary layer on a semi-infinite heated vertical plate (Gebhart and Mahajan 1975). This is a similar character to the start-up flow, although the critical values do vary.

In the remainder of the paper the numerical method is briefly described and the results are presented. Next, a discussion is presented in which the relation of the instability of the boundary layer to possible bifurcation and unsteadiness of the long time flow is considered, then the conclusions are presented.

Numerical method

The Navier–Stokes equations, together with the temperature equation, are expressed in nondimensional form in Cartesian coordinates (x, y) with corresponding nondimensional velocity components (U, V), pressure P, and temperature T as follows:

$$U_t + UU_x + VU_y = -P_x + (U_{xx} + U_{yy}),$$

$$V_t + UV_x + VV_y = -P_y + (V_{xx} + V_{yy}) + \frac{\mathrm{Ra}(T - T_m)}{\mathrm{Pr}},$$

$$U_x + V_y = 0,$$

$$T_t + UT_x + VT_y = \frac{1}{\mathrm{Pr}}(T_{xx} + T_{yy}) + \mathrm{Pert}$$

where subscripts indicate partial differentiation, and the Boussinesq assumption for buoyancy has been made. The Rayleigh number is defined in the notation, length is nondimensionalised by H, the temperature relative to the mean temperature by ΔT, and time by H^2/ν.

Pert is the perturbation added to the flow to allow the stability analysis to be carried out. Pert is zero in most of the domain except for a small $\sim .01 \times .01$ region at the base of the hot wall, where it is set equal to the desired signal. For the random perturbation, Pert = (rand(0) − .5)*10, with rand(0) the standard unix FORTRAN random number generator, generating numbers in the range $0 \leq \mathrm{rand} \leq 1$. For the single-mode perturbation Pert = (sin($2f\pi$), where f is the frequency of the signal. Tests have been conducted to ensure that the perturbation source amplitude is such that the boundary-layer response is in the linear range.

The equations are discretised using an implicit second-order time accurate method defined on a nonstaggered mesh in which all the variables are stored at the same grid locations. All second derivative, pressure gradient, and divergence terms are approximated using second-order centred differences (Armfield 1991, 1994). The advective terms are approximated using QUICK (Leonard 1979). A poisson pressure correction equation, similar to that of the SIMPLE schemes, is used to enforce continuity and obtain the pressure. The grid scale oscillation in the pressure that can occur with nonstaggered grids is prevented by the inclusion of additional elliptic correction terms into the continuity equation. The additional terms are second order and have been shown to have negligible effect on the accuracy of the solution (Armfield 1994).

The domain is discretised using 128 points in the x direction and 128 points in the y direction, with grid stretching being used to concentrate points in the region of the boundary layers and the top and bottom boundaries. The time-step used is $\Delta t = 5 \times 10^{-6}$. It has been shown previously by comparison with experimental data that the basic features of the transient flow can be predicted accurately using an 80×80 mesh (Patterson and Armfield 1990; Armfield and Patterson 1992). Additional grid dependency tests for the present flow were carried out by obtaining results for a single mode ($f = 5000$) on a range of grids (100×100, 128×128, 200×200, 256×256). For each of these grids, the critical height at which this mode became unstable and the amplification at midheight were obtained and compared. The critical height was the most sensitive parameter, and there was found to be a variation of 20% from the 100×100 grid to the 128×128 grid and a variation of 10% from the 128×128 grid to the 256×256 grid. The variation in the amplification was negligible, and it was noted that the basic features of the flow were reproduced on the 100×100 grid, and, thus, it was considered that the 128×128 grid would provide adequate resolution.

Boundary values are specified for the four sides of the domain as follows. The pressure on all the boundaries is obtained by means of a second-order extrapolation from the interior of the domain. All boundaries are nonslip, the top and bottom boundaries are insulated, while the left and right vertical boundaries are set to $\Delta T/2$ and $-\Delta T/2$, respectively.

Results

Results have been obtained for $\mathrm{Ra} = 6 \times 10^8$, 1×10^8, and 6×10^7 all with $\mathrm{Pr} = 7.5$ in a square cavity. Initially, the fluid in the cavity is stationary and isothermal at $T = 0$. At time $t = 0$, the left and right walls are instantaneously heated and cooled to $\Delta T/2$ and $-\Delta T/2$, respectively. Temperature contours for the early part of the transition flow at time $t = 0.003$ for $\mathrm{Ra} = 6 \times 10^8$ are shown in Figure 1, with the intrusions and travelling waves identified on the figure. The waves shown are part of the second set, which are generated by the intrusion striking the base of the hot wall and the top of the cold wall. The waves travel in the downstream direction (up the hot walls and down the cold wall). Owing to the symmetry of the flow, subsequent discussion considers only the hot wall. At this stage of the flow development, the interior of

Notation

g	gravity
H	height of the cavity
Pr	Prandtl number
Ra	Rayleigh number $= g\beta\Delta T H^3/\nu\kappa$
T_m	ambient temperature in cavity
ΔT	total temperature variation in cavity

Greek

β	coefficient of thermal expansion
κ	thermal diffusivity
ν	kinematic viscosity

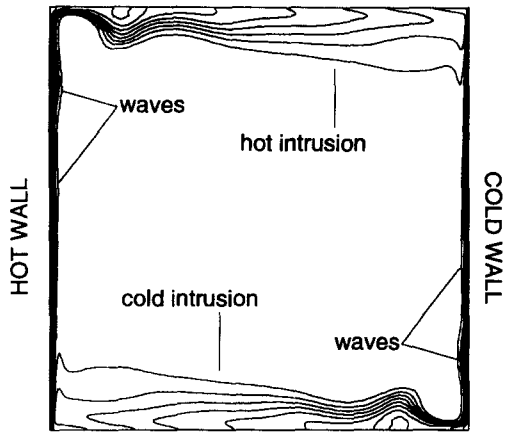

Figure 1 Temperature for the initial solution at $t=0.003$, with intrusions and boundary-layer waves marked

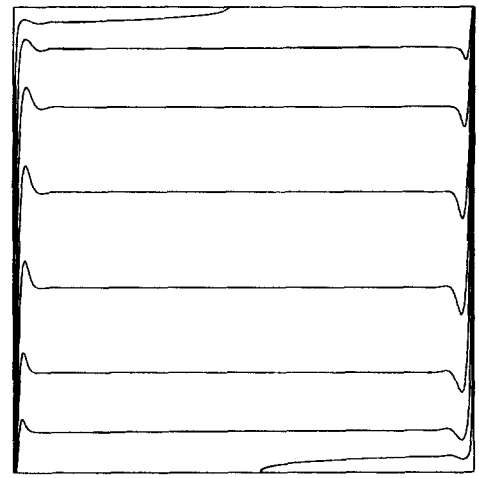

Figure 2 Temperature contours for the steady-state solution at $t=0.5$

the cavity is filled with fluid at ambient temperature. The thermal boundary boundary layer entrains fluid from the interior of the cavity over most of its height, ejecting fluid only over the upper 10%, to form the hot intrusion.

Figure 2 shows the temperature contours for the steady-state $\mathrm{Ra} = 6 \times 10^8$ flow, showing that the interior of the cavity has now filled with linearly stratified fluid. The thermal boundary layer entrains fluid from the interior of the cavity over approximately the lower half of the wall and ejects fluid over the upper half.

In Figure 3, the temperature time series in the boundary layer adjacent to the hot wall at three vertical locations for the transient and steady-state flows are shown. The two sets of travelling waves discussed above are seen in the transient results. No wave activity is seen in the steady-state results.

Figures 4 and 5 compare the temperature and velocity profiles in the boundary layer for the initial and steady-state flows at three vertical locations. The profiles for the initial flow were obtained just prior to the passage of the second set of travelling waves; that is, at time $t = 0.0015$ for the $y = 0.25$ location, $t = 0.0018$ for the $y = 0.5$ location, and $t = 0.0021$ for the $y = 0.75$ location. The width of the temperature boundary layer and the slope at the wall is approximately the same in both the start-up and steady-state flows. However, the total temperature variation is considerably more for the steady-state flow at $y = .25$ and considerably less at $y = .75$ as a result of the stratification in the interior. It is also observed that the profile approaches the interior temperature uniformly for the initial flow, but nonuniformly for the steady-state flow, with a minimum located at approximately $x = .025$ for the three locations. This is an indication that the fluid in the outer part of the boundary layer is being accelerated predominantly by viscous forces rather than buoyancy. Cooler fluid is then lifted above its position of neutral buoyancy, leading to the observed dip in the temperature profile for the steady-state flow. A similar process occurs in the start-up flow, but as there is no stratification of the core fluid, no dip results.

In the velocity profiles, again, the character is approximately the same for the two flows, however considerable differences in detail are apparent. The steady-state profiles are uniformly smaller than the start-up profiles, with the variation increasing with height. Another difference is that the peak velocity in the steady-state profile reduces from the midheight to the $y = 0.75$ location; it increases considerably over this region in the start-up flow. The smaller profile for the steady-state flow is again a result of the stratification, which increases the stability of the core fluid. The reduction in the steady-state profile after the midheight occurs because the boundary layer is then de-entraining fluid, again as a result of the stratification.

A random perturbation was included in the flow at the base of the hot wall, as described in the numerical method section. The resultant temperature time series adjacent to the hot wall at a range of vertical locations are shown in Figure 6. For the lowest three vertical locations, the amplitude of the perturbation appears to be uniformly decaying. After that, some growth is seen in the signal, with the growth apparently being confined to a small band of frequencies, resulting in at the highest location a regular signal with a clearly demarcated frequency band. Clearly, a critical height occurs at around the $y = 0.1$ location, above which at least some of the modes in the random signal become unstable.

Spectral results for the steady-state flow with the random perturbation included, obtained at a range of vertical locations adjacent to the hot wall, are shown in Figure 7. These results were obtained using 16,384 sample points at each y location, with $\Delta t = 5 \times 10^{-6}$, calculating the fast Fourier transform (FFT) and smoothing using a 50-point moving average. Smoothing the FFT allows the general trend of the data to be readily discerned, although, of course, the result cannot be used to obtain the behavior of individual modes. The vertical location of each of the time series is given in the figure caption. Initial decay for all modes is seen from $y = 0.042$ to $y = 0.084$ (Figures 7a–b). However, by $y = 0.125$ (Figure 7c), a very small band of frequencies has started to grow, in the region $5000 \leq f \leq 6000$. Again, clearly, the critical height must lie in the region of $y = 0.1$ and the critical frequency in the range $5000 \leq f \leq 6000$. To identify more accurately the critical frequency that is first to become unstable,

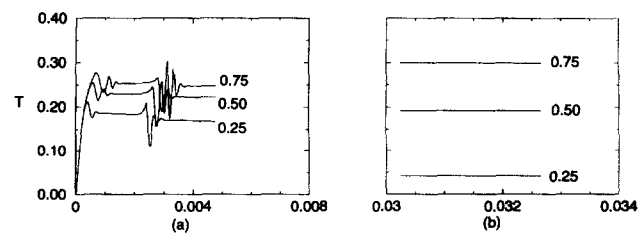

Figure 3 Temperature time series adjacent to the hot wall at $x = 8.3 \times 10^{-3}$ with y locations indicated on the graphs, with time on the horizontal axis, for the initial flow (a), and the steady-state flow (b)

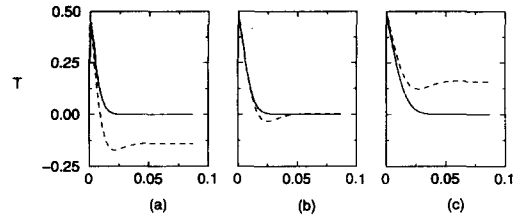

Figure 4 Lateral temperature profiles adjacent to the hot wall at (a) $y=0.25$, (b) $y=0.5$, and (c) $y=0.75$ during the initial flow (solid line) and steady-state flow (dashed line), with distance from the wall on the horizontal axis

a detailed examination of the variation of perturbation amplitude with height for a range of single-mode frequencies was carried out (as shown in Figure 9), with frequency intervals of $\Delta f = 200$ and intervals on the wall of $\Delta y = 0.10$. In this way, it was possible to identify the frequency to first becomes unstable as $f = 5800$ at a critical height of $y = 0.09$. As the signal travels up the wall, the bandwidth of the amplifying modes increases, so that by $y = 0.375$ (Figure 7i), all the modes in the range $4000 \leq f \leq 6000$ are unstable. As the signal continues to travel up the wall, the spectra become strongly peaked, and it is also apparent that the most strongly amplifying mode is shifting to the left, resulting in the strong peak seen at $f = 5000$ at the $y = 0.75$ location (Figure 7l).

The most strongly amplifying mode at the midheight on the wall was obtained in a similar way and found to be $f = 4200$. This is to the left of the peak in the spectra, even at the highest location shown. The spectra represent the integral of the mode over the height of the wall up to the point at which the spectra are shown, and thus the location of the peak is not an accurate indication of the most strongly amplifying mode at that height. Figure 8 contains the time-series for the $f = 4200$ case. The initial decay and growth of the signal is quite clear. The time-series for the critical mode $f = 5800$ is similar to Figure 8, for brevity this graph is not included.

A plot of the perturbation, amplitude against height is given in Figure 9 for both the $f = 5800$ and $f = 4200$ modes. The initial decay and growth of both modes is quite clear with, as noted above, the critical height for $f = 5800$ occurring at $y = 0.09$, and for $f = 4200$ at $y = 0.1$. It is also apparent that at the midheight location the $f = 4200$ mode is growing more strongly than the $f = 5800$ mode. Both modes eventually restabilise, with the $f = 5800$ mode restablising at a smaller y.

Results have also been obtained for $\mathrm{Ra} = 1 \times 10^8$ and $\mathrm{Ra} = 6 \times 10^7$, both again at $\mathrm{Pr} = 7.5$, to allow the variation in the character of the instability with respect to cavity Rayleigh number to be investigated. It should be noted that attempts to further extend the Rayleigh number range were unsuccessful. At Rayleigh numbers lower than 6×10^7, it became very difficult to discern

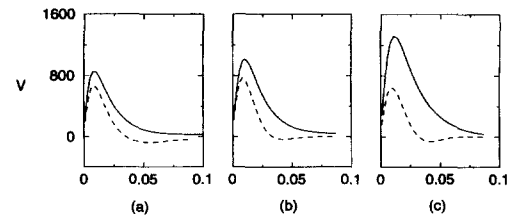

Figure 5 Lateral vertical profiles adjacent to the hot wall at (a) $y=0.25$, (b) $y=0.5$, and (c) $y=0.75$ during the initial flow (solid line), and steady-state flow (dashed line), with distance from the wall on the horizontal axis

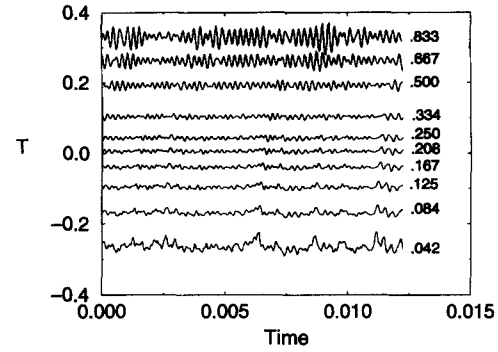

Figure 6 Temperature time series adjacent to the hot wall at $x = 8.3 \times 10^{-3}$ with y locations indicated on the graph for the steady-state flow with the inclusion of random forcing

transition points owing to the low amplification. At Rayleigh numbers much greater than 6×10^8, extremely fine meshes are required, additionally, the movement of the critical point very close to the inflow corner means that inflow effects will be likely to have a major influence on the solution behaviour.

The overall behaviour of the lower Rayleigh number flows are similar to the 6×10^8 flow, and detailed results are not presented. A comparison of y_{cr}, Ra_{cr}, and f_{cr} for each of the Rayleigh numbers is presented in Table 1 with y_{cr} the height at which a single mode first becomes unstable, Ra_{cr} the Rayleigh number based on that height and the cavity temperature difference, and f_{cr} the frequency of the mode that first become unstable. The critical Rayleigh number is also given in a corrected form in which it is based on twice the local temperature difference in the boundary layer. The frequency is also given in the characteristic form $f_{cr}((\mathrm{Pr}/\mathrm{Ra}))^{2/3}$, as suggested by Gebhart and Mahajan (1975). (Gebhart and Mahajan suggested $[f\nu^{1/3}/(g\beta\Delta T)^{2/3}]$ based on a dimensional f and with ΔT the total temperature variation in the boundary layer. $f_{cr}((\mathrm{Pr}/\mathrm{Ra}))^{2/3}$ is an equivalent expression based on the nondimensional f used here and the total temperature variation in the cavity). As can be seen, the critical Rayleigh numbers show a variation of a factor of about two, although this is reduced slightly when the local temperature difference is used. It is to be expected that a variation in the critical Rayleigh number would result from a change in the cavity Rayleigh number, as the cavity flows at different Rayleigh numbers are dissimilar. Additionally, the change in critical height will lead to a difference in the flow structure at that height, which could also be expected to alter the critical Rayleigh number. The characteristic frequency $f_{cr}((\mathrm{Pr}/\mathrm{Ra}))^{2/3}]$ also shows some variation between the $\mathrm{Ra} = 6 \times 10^8$ and the other two results, with a total variation of about 20%.

Discussion

Stability characteristics

The stability characteristics of the thermal boundary layer for the start-up flow were investigated in detail in Armfield and Patterson (1992). In that investigation a one-dimensional (1-D) set of stability equations were constructed by perturbing a base flow solution and dropping all higher-order terms. The resulting equations were similar to the Orr–Sommerfeld equations. The base flow solutions were obtained both directly from the numerical solution, and by using a 1-D error-function solution. Additionally, direct measurements of the numerical solution were carried out. The parameters that were considered to characterise

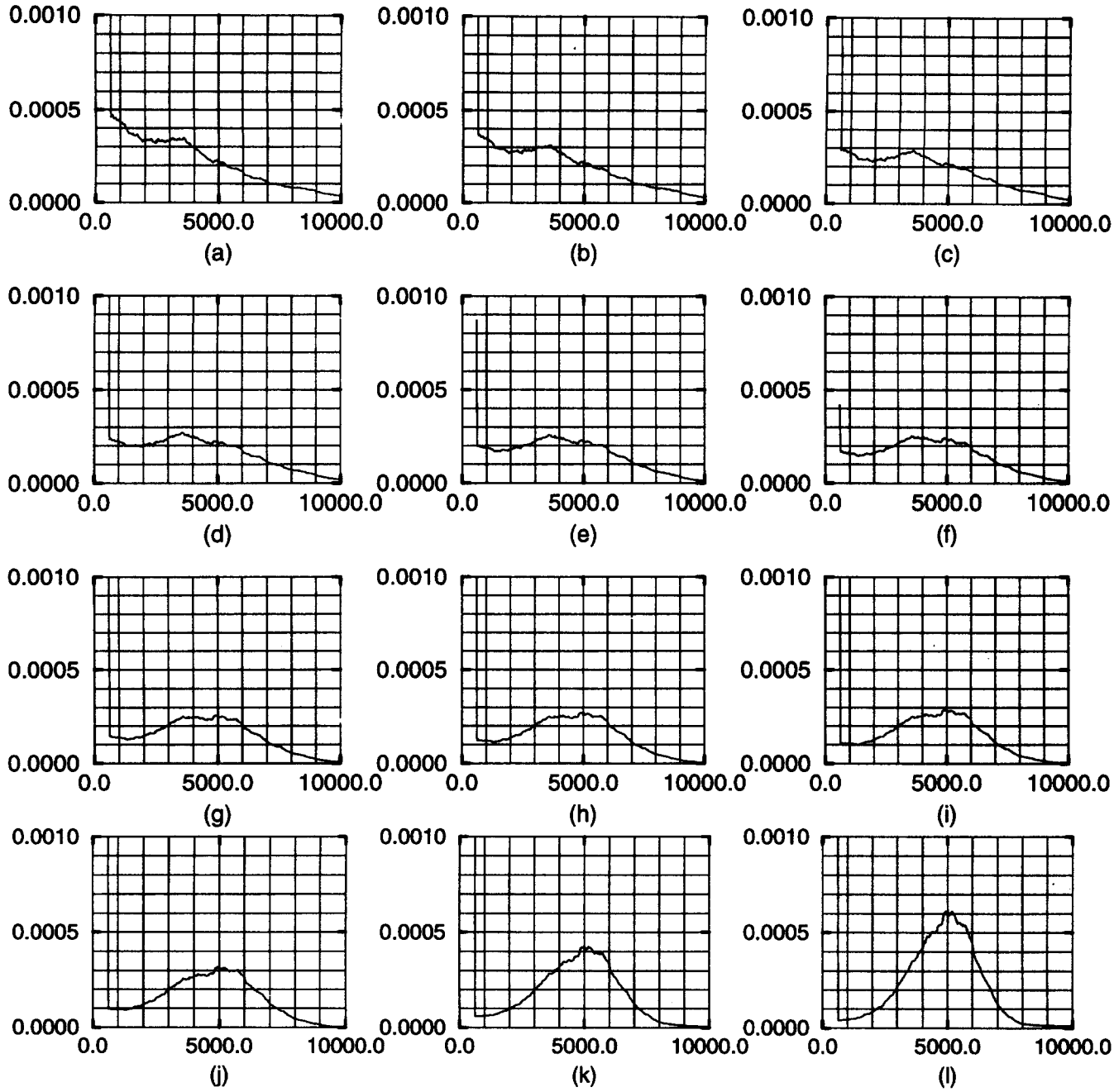

Figure 7 Spectra for the temperature time series at $x=8.3\times10^{-3}$, with frequency (cycles/time) on the horizontal axis for y locations (a) $y=0.042$, (b) $y=0.084$, (c) $y=0.125$, (d) $y=0.167$, (e) $y=0.21$, (f) $y=0.25$, (g) $y=0.29$, (h) $y=0.333$, (i) $y=0.375$, (j) $y=0.420$, (k) $y=0.583$, and (l) $y=0.75$ for the steady-state flow with random forcing

Table 1 Stability characteristics for steady flow

Cavity Ra	y_{cr}	Ra_{cr}	Ra_{cr} (corrected)	f_{cr}	$f_{cr}\left(\frac{Pr}{Ra}\right)^{2/3}$
6×10^8	0.09	4.3×10^5	6.8×10^5	5800	0.031
1×10^8	0.19	6.8×10^5	9.6×10^5	1520	0.027
6×10^7	0.25	9.3×10^5	1.27×10^6	1000	0.025

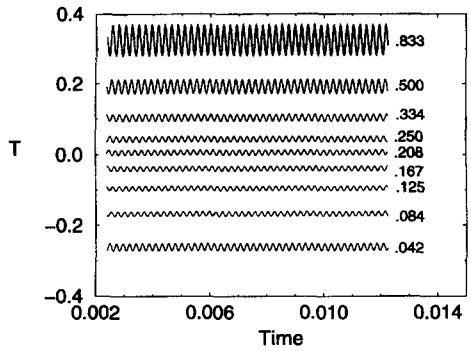

Figure 8 Temperature time series adjacent to the hot wall at $x = 8.3 \times 10^{-3}$ with y locations indicated on the graph for the steady-stage flow with the inclusion of resonant forcing at $f = 4200$

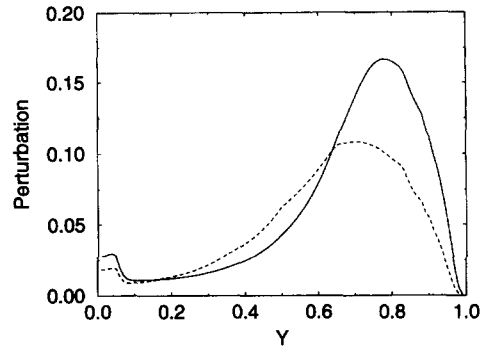

Figure 9 perturbation amplitude against nondimensional height for the critical frequency $f = 5800$ (dashed line) and the most amplified frequency at midheight $f = 4200$ (solid line)

the stability behaviour of the boundary layer were the frequency, velocity, and amplification factor of the maximally amplified component at midheight on the cavity wall, and the critical Rayleigh number, corresponding to the height at which a single mode first became unstable. These parameters were designated f_{max}, v_{max}, A_{max}, and Ra_{cr}, respectively.

In the present paper, these parameters have been obtained for the vertical boundary layers in the steady-state cavity flow, by including a perturbation in the solution at the base of the hot wall and analysing the temperature time series obtained at monitor points at a range of heights adjacent to the hot wall. The distance of the monitor point from the wall has been chosen to give the smallest critical height at which a single mode first becomes unstable. The temperature time series at monitor points is readily collected experimentally by the use of fixed thermistors (Patterson and Armfield 1990), and was thus considered an appropriate quantity for the present analysis.

Considering only the $Ra = 6 \times 10^8$ case, for which the most detailed results have been presented, and which may be compared to the results obtained for the start-up flow in Armfield and Patterson (1992). The amplification factor for the maximally amplifying component at midheight, identified above as $f_{max} = 4200$, is $A_{max} = 4280$. The amplification A is defined by the expression $\exp(A\,\Delta t) = \tau$, where Δt is the time for the wave to travel $\Delta y = 0.1$ and $\tau = [\Delta T'(y + \Delta y)/\Delta T'(y)]$ with $\Delta T'$ the perturbation amplitude. A comparison of the results obtained in Armfield and Patterson for the start-up flow, and the results obtained here for the steady-state flow, is given in Table 2, where here the critical Rayleigh number for the steady-state flow is based on twice the local temperature difference in the boundary layer; i.e., the corrected critical Rayleigh number given in Table 1. The ratio of the wave velocity v_{max} to the peak advection velocity at midheight in the boundary layer is 1.20; whereas, the ratio of v_{max} to the peak advection velocity for the initial flow is 1.02. As noted above, the critical component that first becomes unstable, at $y = 0.09$, has a frequency $f = 5800$, considerably greater than the frequency of the maximally amplifying component at midheight. It is of interest to note that for $f = 5{,}800$ at the midheight the amplification factor is $A = 2107$, and the wave velocity is $v = 750$. It is clear that the two flows have approximately the same stability character. Overall, the steady-state boundary layer is more unstable than the start-up boundary layer, with a larger maximum amplification at midheight and a smaller critical Rayleigh number.

For both the start-up and the steady-state flow, the maximally amplifying frequency at the midheight is less than the critical frequency to first become unstable. The critical frequency to first become unstable for the start-up flow was not given in Armfield and Patterson (1992) but is easily obtained from the results presented there and is included in Table 2. It should be noted that the critical Rayleigh number for the start-up flow given in Armfield and Patterson was obtained by converting a critical time obtained from a stability analysis of the one-dimensional error function solution to a height on the wall by comparing the error function temperature field at that time with the two-dimensional (2-D) temperature field obtained from the numerical solution. This produced a critical Rayleigh number considerably larger than that obtained by a one-dimensional (1-D) stability analysis of the 2-D similarity solution for the semi-infinite isothermal plate, for which $Ra_{cr} = 2.4 \times 10^5$ (Nachtsheim 1963). Recent work in which a direct stability analysis of the isothermal plate has been carried out has verified the critical Rayleigh number given in Armfield and Patterson. The relatively low value obtained by carrying out a 1-D stability analysis of the similarity solution may in part be a result of nonparallel effects.

The boundary layer for both flows has a strongly banded stability character, whereby only those frequency components in a small band around the maximally amplifying component at any height are unstable. When this is combined with the shift in frequency of the maximally amplifying component, and thus the unstable band, to lower frequencies, it is possible for unstable components to become stable as they travel up the wall. However, this variation in the maximally amplified component is small with respect to the change in height, which is an important feature of the flow, because it means that components that become unstable remain unstable for quite some time. Additionally, the total unstable band; that is, those components that were unstable at any height, is quite narrow at these Rayleigh numbers. If this were not the case, the boundary layer would not exhibit the selective amplification feature.

Table 2 Comparison of stability characteristics for initial and steady-state flows

Flow	f_{max}	v_{max}	A_{max}	Ra_{cr}	f_{cr}
Initial	4761	1200	3600	2.7×10^6	6200
Steady-state	4200	936	4280	6.8×10^5	5800

Cavity flow bifurcation

It is well known that a bifurcation with a single mode associated with the boundary layers will occur for the $Pr = 0.71$ flow in a square cavity with insulated horizontal walls at $Ra \sim 2 \times 10^8$ (LeQuéré and Alziary de Roquefort 1985). No such single-mode bifurcation has been observed for the $Pr \sim 7$ flow in a square cavity with adiabatic top and bottom. A bifurcation has been observed for the square cavity at $Pr = 7$ with conducting top and bottom; however, this is associated with a Rayleigh/Bernard instability of the horizontal flow rather than a boundary-layer instability.

LeQuéré (1990) has reported a boundary-layer bifurcation of the $Pr = 7$ flow with an aspect ratio height/width = 10 and insulated horizontal walls at a Rayleigh number $8.4 \times 10^9 < Ra < 9 \times 10^9$ (note LeQuéré's Rayleigh numbers were based on the cavity width; whereas, the Rayleigh number used here is based on the cavity height). In this case, the boundary layer waves are clearly visible, as noted by the author, travelling around the downstream corner, across the horizontal part of the flow, and into the opposite boundary layer.

It is clear that the critical Rayleigh number for the instability of the vertical boundary layer for $Pr = 7$, in the long time cavity flow, is not a good predictor of the critical Rayleigh number for the occurrence of a cavity bifurcation associated with the boundary-layer instability. It has been shown that the steady-state cavity boundary layers have a critical Rayleigh number of $Ra_{cr} \sim 1 \times 10^6$. Thus, for the $Ra = 6 \times 10^8$ case, although the flow on 90% of the vertical walls is unstable, the flow is still nonoscillatory. As noted above, at present no single-mode bifurcation of the square cavity flow for $Pr \sim 7$ with insulated top and bottom has been observed for any Rayleigh number. For high Rayleigh numbers ($Ra > 10^{10}$), unsteady, long time flows have been obtained; however, the flow at such high Rayleigh numbers appears to undergo a sudden broad band transition to an apparently chaotic flow, rather than a bifurcation to a periodic or quasi-periodic flow, as might be expected (Janssen and Henkes 1995). Additionally, mesh-independent solutions have not been obtained for these unsteady, high Rayleigh number flows, and as a result, an accurate critical Rayleigh number for transition to unsteady flow has not been determined.

The reason that the instability of the boundary layer does not necessarily lead to a bifurcation of the cavity flow is that the boundary layer is convectively unstable; whereas, the cavity bifurcation is associated with an absolute instability. A convectively unstable system is one in which an imposed perturbation will exhibit a spatial growth; in this instance, the perturbation leads to waves that travel in the downstream direction on the boundary layer and grow as they travel. If the perturbation is removed, the waves dissipate, and the flow becomes steady, and, thus, to maintain the wave-like nature of the system, the perturbation must be continually imposed. An absolutely unstable system is one which exhibits an unsteady oscillating solution without the continual imposition of a perturbation, such as is observed for the $Pr = 0.71$ cavity flow.

The convective instability of the boundary layer might lead to an absolute instability of the cavity flow if some mechanism in the cavity acts to feed the wave energy exiting the boundary layer at the downstream end back into the upstream end of the boundary layer. If, for example, the travelling waves were able to exit the top of the hot boundary layer, travel across the horizontal region of the flow, and enter the upstream end of the cold boundary layer, and similarly at the downstream end of the cold boundary layer, then we could expect to see a bifurcation. If we further assumed that the waves travelled across the horizontal region without any amplification or dissipation, then it is clear that a bifurcation would occur when a single mode experiences a net amplification in the boundary layer; that is, the total amplification in the unstable downstream region is greater than the total dissipation in the stable upstream region.

Such a bifurcation would still not occur at the critical Rayleigh number for the boundary layer, because at that Rayleigh number, the entire boundary layer is dissipative. For the dissipation in the stable part of the boundary layer to be exactly balanced by the amplification in the unstable part, it is clearly necessary that the Rayleigh number based on the cavity height must be considerably greater than the critical Rayleigh number. Additionally, the feedback mechanism may itself be dissipative, requiring the Rayleigh number to be higher still.

In the high aspect ratio cavity, in which a bifurcation has been observed as noted above, the vertical walls are close enough together so that the horizontal flow is modified, and wave energy can travel across the horizontal flow region from the downstream end of one boundary layer to the upstream end of the other. This is quite clear in the figures presented in LeQuéré (1990) and is noted by the author. The author also notes that the thermal boundary layers for the high aspect ratio cavity are similar to the boundary layers for the square cavity, and, thus, the stability characteristics of the boundary layers in the high aspect ratio cavity will be similar to those for the square cavity. The high aspect ratio flow, thus, satisfies the requirements given above for the occurrence of an absolute cavity instability as a result of the convective boundary-layer instability. The convectively unstable boundary layers are combined with a feedback mechanism to produce an absolute instability of the cavity flow, and the critical Rayleigh number for the cavity flow is then several orders of magnitude greater than the critical Rayleigh number for the boundary layers.

For the square cavity at $Ra = 6 \times 10^8$, $Pr = 7.5$ and insulated top and bottom considered here, there is apparently no such mechanism. The downstream end of the boundary layer together with the horizontal flow are strongly dissipative to the boundary-layer travelling waves. Thus, no energy from the downstream end of one boundary layer travels across to the other boundary layer. Similarly, no wave energy is fed back directly from the downstream end of one boundary layer to its own upstream end. With no feedback mechanism, the convective instability of the boundary layer cannot result in an absolute instability of the cavity, and, thus, no bifurcation can occur.

If the Rayleigh number for the cavity is large enough, then even the input of very small perturbations into the boundary layer, such as those associated with numerical round-off, will be amplified to such an extent that an unsteady flow is produced. Because a total amplification of only an order of magnitude is obtained over the height of the cavity for the $Ra = 6 \times 10^8$ flow, it is likely that such a mechanism would require Rayleigh numbers considerably higher than those considered here. The unsteady flows that have been observed in the square cavity at high Rayleigh numbers may result from the purely convective instability in this way.

Conclusions

A direct analysis of the stability of the thermal boundary layers on the vertical walls, for steady-state flow in a cavity with a horizontal temperature gradient and insulated top and bottom, was carried out. The analysis consisted of introducing a controlled perturbation at the base of the hot wall. The boundary layer was able to support travelling wave solutions, and, thus, the perturbation led to a wave train travelling in the downstream direction. Both random and single-mode perturbations were input. Time series of the temperature adjacent to the hot wall at a range of vertical locations allowed detailed results for the stability characteristics to be obtained. The purpose of the analysis was to determine the stability characteristics of the thermal boundary

layer for the steady-state flow and compare it to the stability characteristics of the thermal boundary layer for the equivalent start-up flow, which were obtained and presented in Armfield and Patterson (1992).

Both flows were observed to have similar stability characteristics, with the primary difference being the increased instability of the steady-state flow. The steady-state flow has a smaller critical Rayleigh number, lower critical frequency, and maximally amplifying frequency at midheight and larger amplification factors.

Despite the instability of the boundary layer for the steady-state flow, no bifurcation or unsteadiness of the long time flow is observed. It is hypothesised that a bifurcation will only occur if the convective instability of the boundary layer is combined with a feedback mechanism of some sort and that the critical Rayleigh number for a bifurcation would be expected to be considerably greater than the critical Rayleigh number for the instability of the boundary layer. Similarly, the convectively unstable boundary layer may lead directly to a broad-band unsteadiness, but this would, again, be at a Rayleigh number much greater than the critical boundary-layer Rayleigh number.

Acknowledgment

The authors wish to acknowledge the support of the Australian Research Council through Australian Research Council grants No. A89231072 and No. A89331991. The authors also wish to acknowledge the suggestions of Messrs. Patterson, Schoepf and Brooker of the Centre for Water Research at the University of Western Australia.

References

Armfield, S. W. 1989. Direct simulation of unsteady natural convection in a cavity. *Proc. Intl. Symposium on Computational Fluid Dynamics*, Nagoya, Japan, North-Holland, Amsterdam, 305–310

Armfield, S. W. 1991. Finite difference solutions of the Navier–Stokes equations on staggered and non-staggered grids. *Computers and Fluids*, **20**, 1–17

Armfield, S. W. 1994. Ellipticity accuracy and convergence of the discrete Navier–Stokes equations. *J. Compt. Phys.* **114**, 176–184

Armfield, S. W. and Patterson, J. C. 1992. Wave properties of natural convection boundary layers. *J. Fluid Mech.*, **239**, 195–211

Gebhart, B. and Mahajan, R. L. 1975. Characteristic disturbance frequency in vertical natural convection flow. *Int. J. Heat Mass Transfer*, **18**, 1143–1148

Janssen, R. J. A. and Henkes, R. A. W. M. 1995. Influence of Prandtl number on instability mechanisms and transition in a differentially heated square cavity. *J. Fluid Mech.*, **290**, 319–344

Leonard, B. P. 1979. A stable and accurate convective modelling procedure based on quadratic upstream interpolation. *Comp. Method. Appl. Mech. Eng.*, **19**, 59–98

LeQuéré, P. 1990. Transition to unsteady natural convection in tall water filled cavities. *Phys. Fluids A*, **4**, 503–515

LeQuéré, P. and Alziary de Roquefort, T. 1985. Transition to unsteady natural convection of air in differentially heated vertical cavities, *Proc. 4th Int. Conference, Numerical Methods in Laminar and Turbulent Flow*, Swansea, Wales, 841–852

Nachtshiem, P. R. 1963. Stability of free convection boundary layers flows. NASA TN D-2089

Patterson, J. C. and Armfield, S. W. 1990. Transient features of natural convection in a cavity. *J. Fluid Mech.*, **219**, 469–497